Journal of Alloys and Compounds 762 (2018) 631–636

Contents lists available at ScienceDirect

Journal of Alloys and Compounds

journal homepage: http://www.elsevier.com/locate/jalcom

Design of diffusion barrier and buffer layers for β-Zn_4Sb_3 mid-temperature thermoelectric modules

Li-Wei Chen, Cheng Wang, Yi-Chia Liao, Chia-Lin Li, Tung-Han Chuang, Chun-Hway Hsueh*

Department of Materials Science and Engineering, National Taiwan University, Taipei 10617, Taiwan

ARTICLE INFO

Article history:
Received 23 January 2018
Received in revised form
19 May 2018
Accepted 21 May 2018
Available online 22 May 2018

Keywords:
Thermoelectric materials
Thin films
Diffusion
X-ray diffraction

ABSTRACT

The purpose of this work was to investigate the feasibility of using sputtered Ti/W-Ti/Ti multilayer as diffusion barrier and buffer layers between β-Zn_4Sb_3 thermoelectric (TE) material and Ag interconnect layer for mid-temperature TE module applications. Interdiffusion at the interface was examined by both scanning electron microscope and Auger electron spectroscopy. After penetrating the Ti buffer layer, Ag, Zn and Sb were successfully blocked by the W-Ti diffusion barrier layer. We also proved that the TE sample with diffusion barrier and buffer layers showed phase stability after high temperature aging. Also, the sheet resistance decreased as the temperature increased and it indicated good electrical properties at high working temperatures. In addition, the solid-liquid interdiffusion method was used to join the TE module, and the bonding remained stable at the TE module working temperature.

1. Introduction

As the public awareness in environmental issues has arisen in recent years, the applications of thermoelectric (TE) modules are becoming widespread for reducing fuel consumption. TE materials convert temperature difference into electrical power through Seebeck effect [1,2]. The conversion efficiency depends on their TE figure of merit (ZT), which can be expressed as $ZT = S^2T\sigma/\kappa$, where S is Seebeck coefficient, σ is electrical conductivity, κ is thermal conductivity and T is average temperature of the hot and the cold plates of the TE module. TE materials are normally classified depending on their temperature ranges of applications. The mid-temperature range is from 200 to 600 °C, which is the temperature range of most industrial waste heat sources [3–8]. Among the wide variety of mid-temperature materials, Zn-Sb system is promising due to its low toxicity and low-cost for fabrication [9]. Specifically, β-Zn_4Sb_3 in this system is stable at room temperature, while it would transfer to ZnSb and Zn due to Zn diffusion during fabrication and transfer back to β-Zn_4Sb_3 when the temperature is above 250–300 °C [10]. Nevertheless, because β-Zn_4Sb_3 has quite low thermal conductivity close to the amorphous limit of below 1 W/mK [11], it possesses a high value of ZT and is worth exploring [12]. However, to make the module functional, the joint between the electrodes and the TE material is another critical issue in addition to the ZT value [13,14].

Generally, traditional soldering was used in dealing with TE joint because the low bonding temperature could prevent thermal cracking during the bonding process [15]. However, the highest operating temperature of TE was limited by the melting point of the solder and soldered TE modules might break down when the working temperature was higher than the melting point of the solder alloy. The optimized operating temperature for the application of β-Zn_4Sb_3 is 400 °C where β-Zn_4Sb_3 possesses the highest ZT value at this temperature [3,5,16–18]. Hence, brazed TE module was of concern because of its melting point while it might result in serious interfacial cracking during solidification of the brazed filler [19]. Currently, spark plasma sintering [20] is the most common way for the joint between TE material and metallic electrodes working in the medium and high temperature ranges to prevent interfacial cracking. However, the high heating rate during the spark plasma sintering would degrade the intrinsic property of mid-temperature β-Zn_4Sb_3. Therefore, spark plasma sintering was not suitable for the β-Zn_4Sb_3 module [21]. In addition to bonding, another issue could occur; i.e., the interdiffusion between the TE material and solder could degrade the device performance because the carrier concentration of the TE material would be changed. The same diffusion problem also occurred in other TE system; e.g.,

* Corresponding author.
E-mail address: hsuehc@ntu.edu.tw (C.-H. Hsueh).

https://doi.org/10.1016/j.jallcom.2018.05.251
0925-8388/

Bi_2Te_3 TE material with In-based solder [13]. Hence, successful joints for TE modules should satisfy both low interdiffusion and good adhesion in the TE system.

To resolve the diffusion problem, a diffusion barrier was required between electrodes and TE materials to enhance the joint reliability and device efficiency [14,22–25]. Thin film metallic glass [26–29] has been adopted as diffusion barrier between Si and Cu [27] and between Cu and Sn [29] in recent years due to its amorphous structure that could efficiently impede diffusion. However, it was found that some element in metallic glasses such as Ni would interact with Zn in β-Zn_4Sb_3 to form Ni_5Zn_{21} intermetallic compound [30]. Hence, refractory elements, such as W and Ti, were considered as the diffusion barrier material in the present study. W-Ti thin films have many attractive properties from the industrial application point of view, such as low electrical resistance, high thermal stability, chemical inertness and good adhesion [31–33]. W-Ti has been commonly used as diffusion barrier [34–38]. Many studies have investigated W-Ti as a barrier layer for Ag, Cu and Al interconnects on Si wafers [35,39–42]. It was reported that W-Ti in contact with Ag, Cu and Al was stable up to 600 °C. However, no research has been performed on W-Ti as the diffusion barrier layer for TE systems.

In this study, an alternative joining technique of solid-liquid interdiffusion (SLID) [19], which was based on the principle of isothermal solidification and interfacial intermetallic reaction, was adopted to overcome the problem of thermal cracking to ensure that the mid-temperature TE module (β-Zn_4Sb_3) could be used under the optimized working temperature of 400 °C [19,43–45]. To resolve the issue of interfacial diffusion between the Ag interconnect layer and β-Zn_4Sb_3, W-Ti as a diffusion barrier layer was adopted in the present study. However, W-Ti film was found to be hard to bond to β-Zn_4Sb_3 in the present study and improvement of adhesion was required. During thin film deposition, Ti thin film has often been used as the adhesive layer [46,47]. Also, Ti has the coefficient of thermal expansion that is less than β-Zn_4Sb_3 and Ag but is higher than W-Ti, and it could mitigate thermal mismatch stresses in the system. Hence, Ti was adopted as the buffer layer in the present study to enhance adhesion between W-Ti layer and adjacent layers (i.e., β-Zn_4Sb_3 and Ag).

2. Material and methods

2.1. Processing of TE material and Ag interconnect with diffusion barrier and buffer layers

β-Zn_4Sb_3 source alloy ingot was obtained from Thermal Management Materials & Device Lab., Industrial Technology Research Institute (ITRI). The source ingot was processed by mechanical grinding with Al_2O_3 milling balls for 18 h and subsequently hot pressing under 60 MPa at 390 °C for 180 s to fabricate the TE bulk material. It was then cut into pieces with a dimension of $0.5 \times 0.5 \times 0.3$ cm^3 each. Prior to deposition of diffusion barrier and buffer layers, the TE materials were cleaned ultrasonically in acetone, ethanol and deionized water for 10 min each in sequence [48]. Small thicknesses of the TE materials were preferred for sputtering deposition of films because ion bombardment would be converted to heat that could not be readily released from TE material to the substrate holder due to the low thermal conductivity of β-Zn_4Sb_3. The chamber was pumped to the base pressure of 5×10^{-7} Torr before the deposition process. After the introduction of the sputtering gas (Ar 99.999%) into the chamber, the working pressure was kept at 4×10^{-3} Torr. The substrate holder was rotated at a speed of 60 rpm with the working distance of 10 cm to maintain uniformity of chemical composition of the coating. The vendor of our sputtering targets was Ultimate Materials Technology Co., Ltd., and W-Ti (30 at.% Ti), Ti (purity 99.99 wt.%) and Ag (purity 99.99 wt.%) targets of 7.6 cm in diameter were used in the three-target DC/RF sputtering system. Ti film of ~1 μm thickness was deposited first on the β-Zn_4Sb_3 TE material by DC magnetron sputtering at a power of 50 W for 4000 s. Then, W-Ti of ~1 μm thickness was deposited at a power of 50 W for 2000 s. After that, Ti was deposited again under the same condition as the first deposition of Ti film. The thickness of 15 μm was usually required for Ag interconnect layer used in SLID bonding process [19]. It would be impractical to deposit such a thick Ag layer using sputtering and electroplating was used instead. However, because of the poor adhesion between Ti film and electroplated Ag, 100 nm Ag was deposited on the top of Ti film by sputtering prior to electroplating. Finally, Ag was deposited by electroplating at a current of 0.02 A for 10 min.

2.2. Characterization of interdiffusion, phase stability and sheet resistance

At the joint interface, interdiffusion was analyzed by scanning electron microscope (SEM, JEOL, JSM-7800F Prime) equipped with energy dispersive spectroscopy (EDS). To examine diffusion across the interfaces in details, the compositional depth profile was obtained using the Auger electron spectroscopy (AES) equipped with an Ar-ion gun for etching. The etching condition was 30.3 nm/min by referring to the etching rate of SiO_2, and the signal collection time per cycle for the sample was 7 s. Because of the slow etching rate of the Ar-ion gun, reduced thickness of the sample was used for AES analyses. In this case, both Ti layers of ~40 nm thickness were

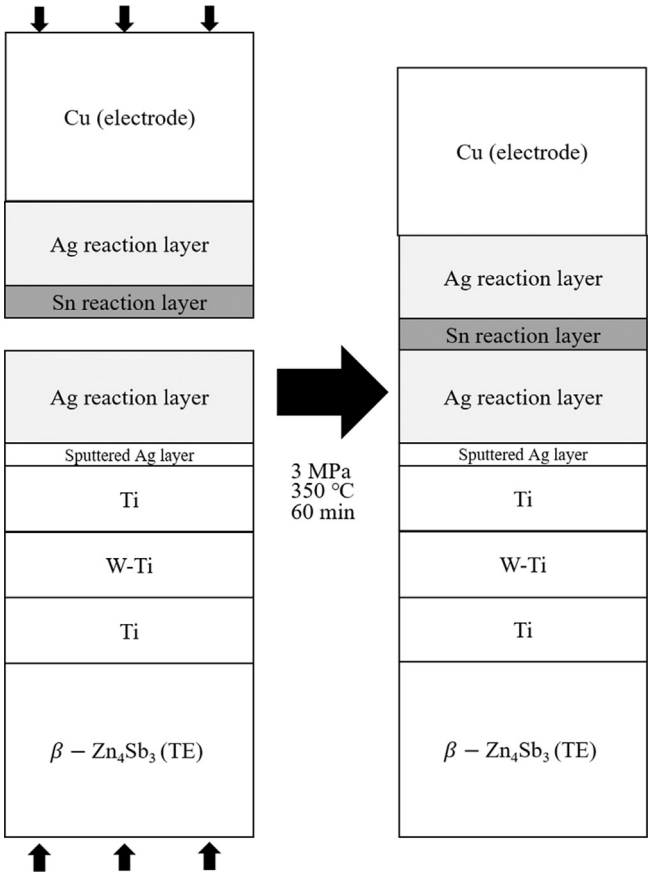

Fig. 1. Schematics showing the SLID joining process for manufacturing β-Zn_4Sb_3 TE module with Ag-based solder and Ti/W-Ti/Ti diffusion barrier and buffer layers.

sputtered at a power of 50 W for 200 s, W-Ti layer of ~60 nm thickness was sputtered at a power of 50 W for 400 s, and Ag of ~100 nm thickness was sputtered on the top of Ti without the electroplated Ag layer.

To examine the phase stability after the aging treatment, X-ray diffraction analysis (Rigaku TTRAX 3) was performed with the voltage and current settings at 50 kV and 300 mA, respectively. All samples were investigated using Cu Kα radiation over a 2-theta angle range of 20–80° with a step size of 0.02° and the measurements were conducted at room temperature after aging treatments. The sheet resistances of the samples were measured by a standard four-point probe method. Samples were prepared at different annealing temperatures, and each datum was the average of four measurements.

2.3. SLID joining process

The TE sample (i.e., β-Zn_4Sb_3/Ti/W-Ti/Ti/Ag) was joined to a Cu electrode using SLID bonding process shown in Fig. 1. Before joining, the Cu electrode was electroplated with a 4 μm-thick Ag layer and an 1 μm-thick Sn layer. The TE sample was assembled with the Sn/Ag-coated Cu electrode in a vacuum furnace of 3.9 $\times 10^{-6}$ Torr and hot pressed at 350 °C for 60 min under a pressure of 3 MPa [19].

3. Results and discussion

3.1. Interdiffusion analyses

To provide the better resolution of the compositional profile to study diffusion at the interface, measurements of AES depth profiles were conducted and the results and their corresponding SEM cross-section micrographs are shown in Fig. 2 for aging at 400 °C for different durations. Without the aging treatment, as-deposited Ag and W-Ti layers were clearly separated by the Ti buffer layer in the depth profile shown in Fig. 2(a), and the interfaces between layers could be readily identified in the corresponding cross-section micrograph shown in Fig. 2(d). After aging at 400 °C for 24 h and 72 h, the intensity of Ti decreased and the Ag and Ti spectra overlapped more with the aging time as shown in Fig. 2(b) and (c). Also, the contrast between Ag and Ti became more difficult to be resolved in Fig. 2(e) and (f). At the interface between β-Zn_4Sb_3 and Ti, the intensities of Zn and Sb did not show obvious change with the aging time; however, the intensity of Ti decreased with the aging time. Although interdiffusion occurred between the Ti buffer layer and the adjacent Ag and β-Zn_4Sb_3, diffusion of Ag, Zn and Sb was blocked by the W-Ti diffusion barrier layer as shown in Fig. 2(b) and (c), where the intensities of Ag, Zn and Sb decreased almost to zero as the intensity of W appeared. Aging at 400 °C for 240 h was

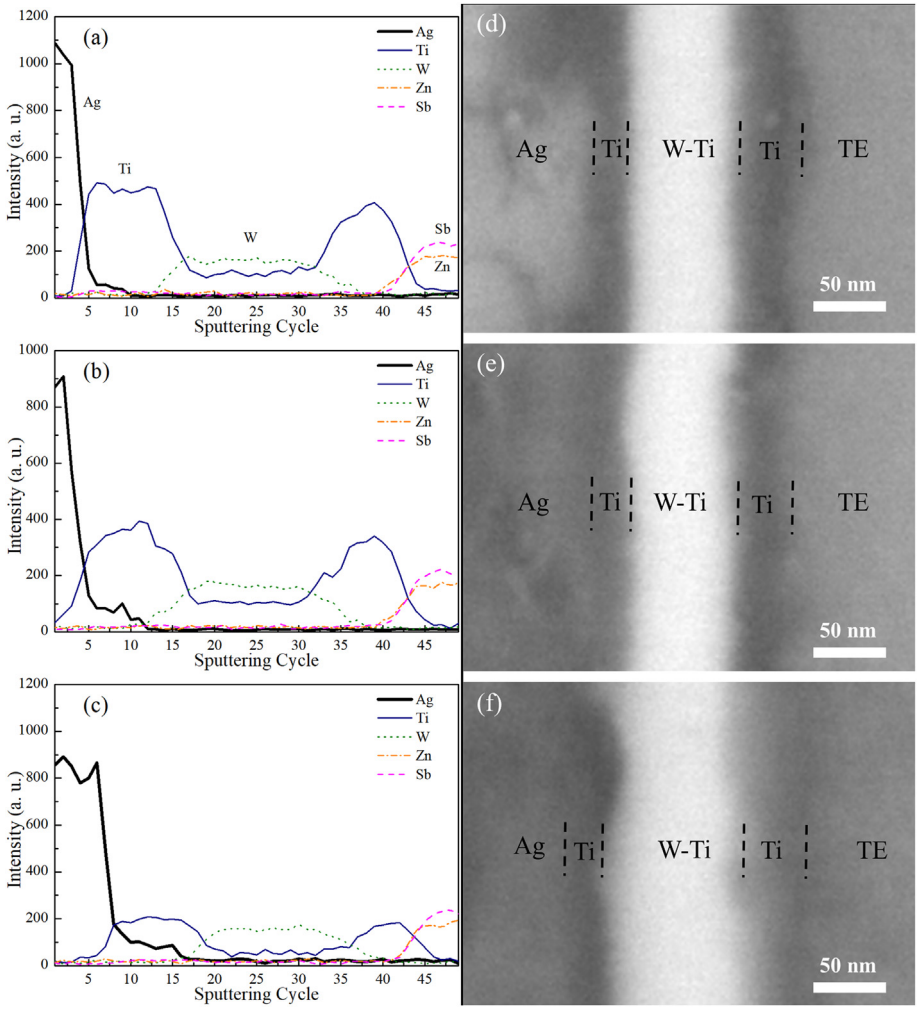

Fig. 2. Auger electron microscopy depth profile of TE sample (β-Zn_4Sb_3/Ti/W-Ti/Ti/Ag) aged at 400 °C for (a) 0, (b) 24 and (c) 72 h and their corresponding SEM cross-section micrographs of TE sample aged at 400 °C for (d) 0, (e) 24 and (f) 72 h. The film thickness of Ti/W-Ti/Ti was about 140 nm.

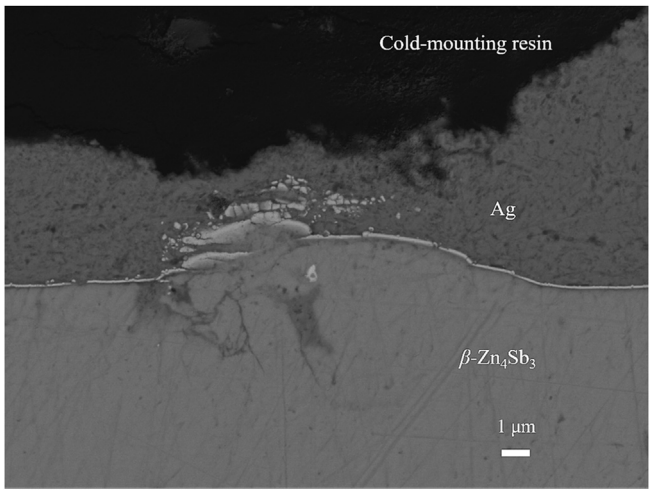

Fig. 3. SEM cross-section image of the TE sample (β-Zn_4Sb_3/Ti/W-Ti/Ti/Ag) in the interdiffusion study using AES depth profile.

also conducted; however, ZnO was found all over the surface from SEM examination and this was due to both the rough surface of β-Zn_4Sb_3 TE material and insufficient thickness of Ti/W-Ti/Ti diffusion barrier and buffer layers used in AES analyses as discussed in the following.

It is worth noting that although the micrograph shown in Fig. 2 exhibits rather smooth surface of β-Zn_4Sb_3 TE material in the local region, the surface roughness of TE material was about 1 μm in the global scale as shown in Fig. 3. While our designed Ti/W-Ti/Ti layer was about 140 nm in our AES interdiffusion study, this thin diffusion barrier/buffer layer was inadequate to fully cover the TE material. As a result, Zn might passed through the site where the TE material was not adequately covered and reacted with oxygen at the sample surface. To avoid this problem, the regular thicker barrier/buffer layer (~3 μm) was also used to study interdiffusion using SEM EDX mapping shown as follows. Also, to reduce the surface roughness of β-Zn_4Sb_3 TE material, electrochemical polishing would be adopted prior to ultrasonic cleaning of the TE material in our future work.

The cross-section of the TE sample β-Zn_4Sb_3/Ti/W-Ti/Ti/Ag used for SEM EDX mapping is schematically shown in Fig. 4(a). After Ti/W-Ti/Ti of ~3 μm thickness was sputtered on β-Zn_4Sb_3, Ag of ~100 nm thickness was then sputtered on the top of Ti/W-Ti/Ti in order to increase the surface electric conductivity to allow the subsequent electroplating of Ag of 15 μm thickness with good bonding. The TE samples were aged at 400 °C for 3 and 10 days, respectively, and the corresponding SEM EDX mappings are shown in Fig. 4(b) and (c). For 3-day aging, Fig. 4(b) shows that Ag, Zn and Sb diffused into the Ti layer; however, they were block by the W-Ti layer. For 10-day aging, Fig. 4(c) shows nearly the same EDX mapping as Fig. 4(b) for 3-day aging. However, Ti and Ag interdiffusion was more obvious in Fig. 4(c). Also, although W has extremely low atomic mobility, its diffusion was more obvious in Fig. 4(c) compared with Fig. 4(b) as W could form solid solution with Ti in its whole composition rang based on the W-Ti phase diagram [49].

It would be of interest to study the mechanism of diffusion of Ag, Zn and Sb into the Ti layer. However, the measurement of penetration depth as a function of diffusion time would be required. While a parabolic relation signifies the diffusion control, a linear relation signifies the interface reaction control. This study could not be achieved using the present results because of the thin Ti layer (1 μm), long annealing time (3 and 10 days) and the penetration of Ag, Zn and Sb through the Ti layer.

3.2. Phase stability

To ensure the phase stability of sputtered films and the TE material, XRD measurements of β-Zn_4Sb_3/Ti/W-Ti/Ti were conducted and the results are shown in Fig. 5. Our designed films kept their original phases from as-deposited to 400 °C aging for 24 h. To increase *ZT* value, control of the carrier concentration of TE materials by means of phase transformation has been adopted [50–52]. While β-Zn_4Sb_3 has the highest *ZT* value in the Zn-Sb system, phase transformation is not required. It is shown in Fig. 5 that β-Zn_4Sb_3 maintained its phase stability from as-deposited to 400 °C aging in the presence of Ti/W-Ti/Ti diffusion barrier and buffer layers.

3.3. Electrical properties

Electrical properties of sputtered diffusion barrier and buffer layers were also examined. Measurements using the standard four-

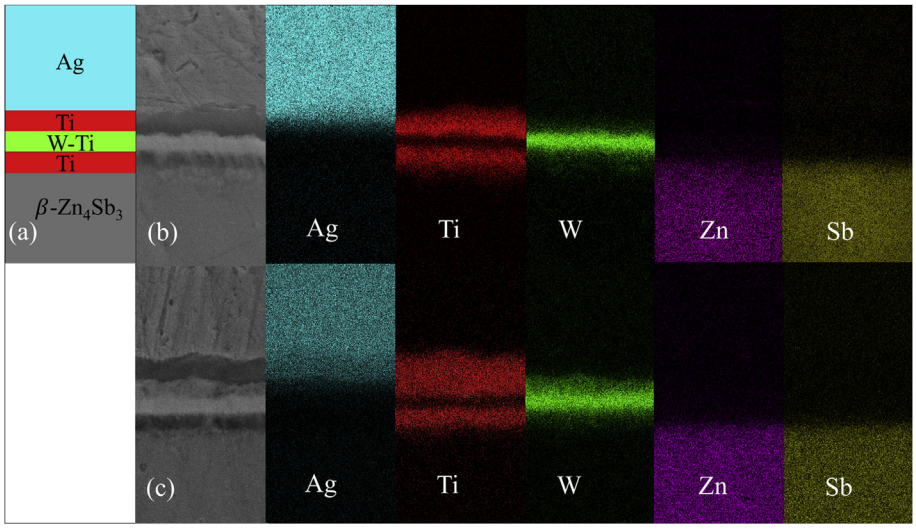

Fig. 4. (a) Schematic illustration of the TE sample (β-Zn_4Sb_3/Ti/W-Ti/Ti/Ag) and SEM EDX mapping of TE sample aged at 400 °C for (b) 3 days and (c) 10 days. Ti/W-Ti/Ti is ~3 μm thick.

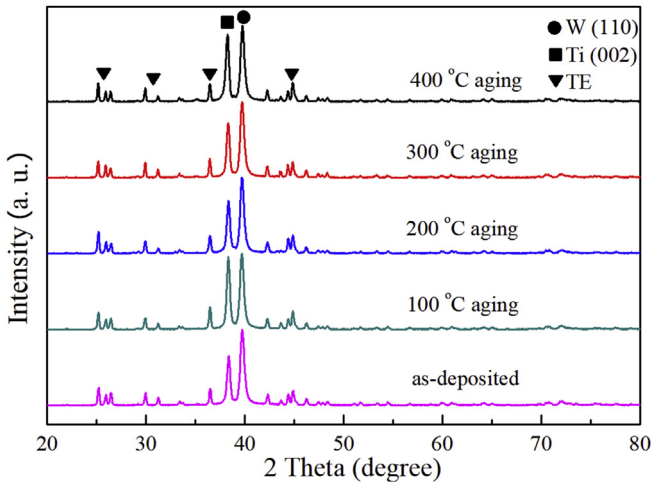

Fig. 5. XRD profiles of β-Zn_4Sb_3/Ti/W-Ti/Ti for as-deposited and samples aged at different temperatures for 24 h.

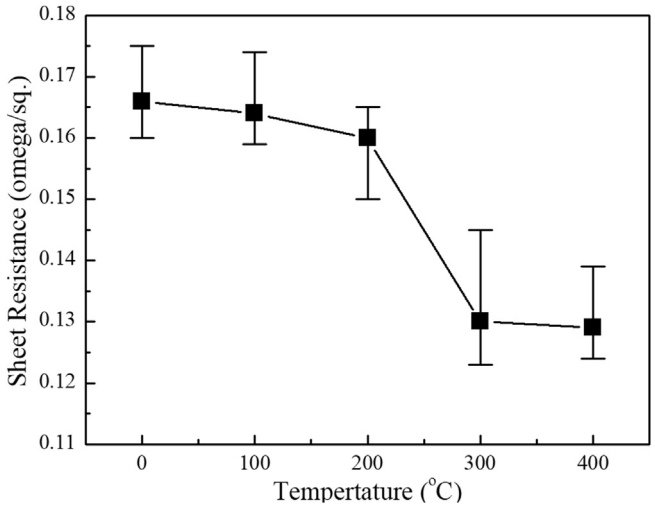

Fig. 6. Sheet resistance of β-Zn_4Sb_3/Ti/W-Ti/Ti versus aging temperature for 24 h of aging.

point probe method were conducted and the results of sheet resistance of β-Zn_4Sb_3/Ti/W-Ti/Ti aged at different temperatures for 24 h are shown in Fig. 6 with measurements conducted four times for each aging temperature. From Fig. 6, there was a decreasing trend of sheet resistance as the aging temperature increased. The increase of aging temperature would result in higher atomic density of sputtered films, where defects were annihilated and the crystallinity of W-Ti film was improved [53]. Therefore, our designed layers would possess better electric properties after aging.

3.4. SLID joining of TE module

To investigate the feasibility of industrial applications, TE sample β-Zn_4Sb_3/Ti/W-Ti/Ti/Ag was bonded to the Cu electrode by the SLID process. The cross-section of the TE module β-Zn_4Sb_3/Ti/W-Ti/Ti/Ag-based solder/Cu without aging is shown in Fig. 7(a). After aging at 400 °C for 24 h, the cross-section was examined using SEM EDX mapping and the result shown in Fig. 7(b) maintained nearly the same compared to the one without aging shown in Fig. 7(a). In Fig. 7(b), Zn, Sb and Ag-based solder were successfully blocked by our designed layers of Ti/W-Ti/Ti. Therefore, our diffusion barrier and buffer layers could successfully prevent interdiffusion. It is worth noting that because Zn has a much lower atomic number (30) than Sb (51), the intensity in EDX line scan of Zn was much lower than that of Sb [54].

4. Conclusions

We successfully demonstrated that sputtered Ti/W-Ti/Ti multilayer could be used as the effective diffusion barrier and buffer layers between β-Zn_4Sb_3 and Ag interconnect for mid-temperature TE module applications. Specifically, SEM EDX mapping showed that Ag, Zn and Sb diffused into Ti buffer layer, while they were blocked by W-Ti diffusion barrier layer after aging at the working temperature of 400 °C for 10 days. XRD results revealed the phase stability of no phase transformation of β-Zn_4Sb_3 in the presence of Ti/W-Ti/Ti diffusion barrier/buffer layers after aging at 400 °C for 24 h. Also, sheet resistance measurements showed improved electric properties as the temperature increased to the working temperature of 400 °C. Finally, TE sample with diffusion barrier/buffer layers was modulized to be bonded to Cu electrode using SLID bonding process, and our diffusion barrier system showed good barrier ability to prevent interdiffusion.

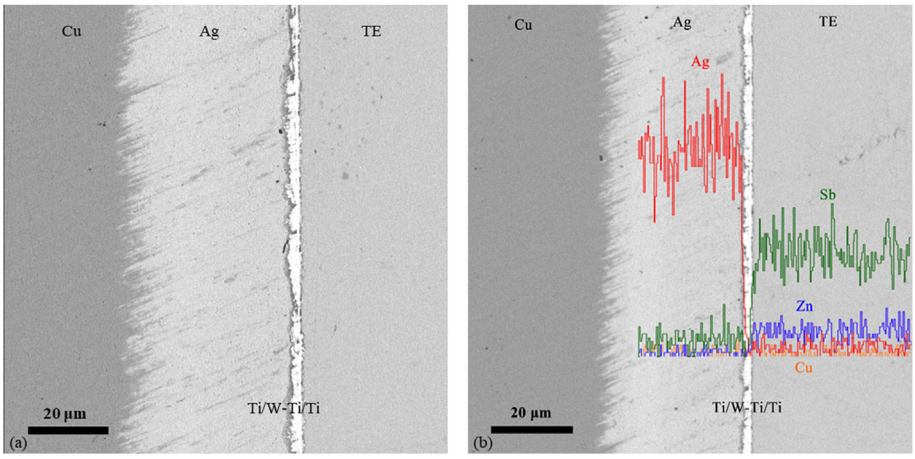

Fig. 7. SEM image of the cross section of TE module after bonding to Cu electrode using SLID process after aging at 400 °C for (a) 0 h and (b) 24 h with EDX line scan.

Acknowledgments

This work was supported by the Ministry of Science and Technology, Taiwan under Contract no. MOST 106-2221-E-002-072-MY2. We thank Prof. C.S. Lin and Ms. Y.T. Lee of Instrumentation Center, National Taiwan University for FEG-SEM experiments.

References

[1] W.P. Lin, D.E. Wesolowski, C.C. Lee, Barrier/bonding layers on bismuth telluride (Bi_2Te_3) for high temperature thermoelectric modules, J. Mater. Sci. Mater. Electron. 22 (2011) 1313–1320.
[2] F. Cheng, Z. Ma, Y. Wang, G. Zhang, W. Long, Microstructure and aging resistance of the joints between SAC305 solder and thermoelectric materials with different diffusion barriers, Kovove Mater. 52 (2014) 157–162.
[3] T. Zou, W. Xie, J. Feng, X. Qin, A. Weidenkaff, Recent developments in β-Zn_4Sb_3 based thermoelectric compounds, J. Nanomater. 4 (2015) 642909.
[4] T. Zhu, X. Zhao, M. Yan, S. Hu, T. Li, B. Zhou, Transport properties of β-Zn_4Sb_3 prepared by vacuum melting, Mater. Lett. 46 (2000) 44–48.
[5] M. Chitroub, F. Besse, H. Scherrer, Thermoelectric properties of semiconducting compound Zn_4Sb_3, J. Alloys Compd. 460 (2008) 90–93.
[6] S.-C. Ur, P. Nash, I.-H. Kim, Solid-state syntheses and properties of Zn_4Sb_3 thermoelectric materials, J. Alloys Compd. 361 (2003) 84–91.
[7] F. Ren, E.D. Case, J.E. Ni, E.J. Timm, E. Lara-Curzio, R.M. Trejo, C.-H. Lin, M.G. Kanatzidis, Temperature-dependent elastic moduli of lead telluride-based thermoelectric materials, Philos. Mag. A 89 (2009) 143–167.
[8] J.E. Ni, E.D. Case, R.D. Schmidt, C.-I. Wu, T.P. Hogan, R.M. Trejo, E. Lara-Curzio, M.G. Kanatzidis, Fracture mode, microstructure and temperature-dependent elastic moduli for thermoelectric composites of PbTe–PbS with SiC nanoparticle additions, Philos. Mag. A 93 (2013) 4412–4439.
[9] F. Tseng, S. Li, C. Wu, Y. Pan, L. Li, Thermoelectric and mechanical properties of ZnSb/SiC nanocomposites, J. Mater. Sci. 51 (2016) 5271–5280.
[10] T. Zhang, K. Zhou, X. Li, Z. Chen, X. Su, X. Tang, Reversible structural transition in spark plasma-sintered thermoelectric Zn4Sb3, J. Mater. Sci. 51 (2016) 2041–2048.
[11] X. Li, J. Carrete, J. Lin, G. Qiao, Z. Wang, Atomistic origin of glass-like Zn4Sb3 thermal conductivity, Appl. Phys. Lett. 103 (2013) 103902.
[12] G.J. Snyder, M. Christensen, E. Nishibori, T. Caillat, B.B. Iversen, Disordered zinc in Zn4Sb3 with phonon-glass and electron-crystal thermoelectric properties, Nat. Mater. 3 (2004) 458–463.
[13] S. Li, D. Yang, Q. Tan, L. Li, Evaluation of electroplated Co-P film as diffusion barrier between In-48Sn solder and SiC-dispersed Bi_2Te_3 thermoelectric material, J. Electron. Mater. 44 (2015) 2007–2014.
[14] H. Li, H. Jing, Y. Han, G.-Q. Lu, L. Xu, T. Liu, Interfacial evolution behavior of AgSbTe 2.01/nanosilver/Cu thermoelectric joints, Mater. Des. 89 (2016) 604–610.
[15] M. Nahavandi, M. Hanim, Z. Ismarrubie, F. Baserfalak, Interfacial reaction of Bi–Ag and Bi–Sb solders on copper substrate with multiple reflow number, Mater. Res. Innovat. 18 (2014). S6–318-S316-321.
[16] T. Caillat, J.-P. Fleurial, A. Borshchevsky, Preparation and thermoelectric properties of semiconducting Zn4Sb3, J. Phys. Chem. Solid. 58 (1997) 1119–1125.
[17] V. Kuznetsov, D. Rowe, Solid solution formation in the Zn_4Sb_3–Cd_4Sb_3 system, J. Alloys Compd 372 (2004) 103–106.
[18] S.C. Ur, I.H. Kim, P. Nash, Thermoelectric properties of Zn_4Sb_3 directly synthesized by hot pressing, Mater. Lett. 58 (2004) 2132–2136.
[19] T.H. Chuang, W.T. Yeh, C.H. Chuang, J.D. Hwang, Improvement of bonding strength of a (Pb, Sn) Te–Cu contact manufactured in a low temperature SLID-bonding process, J. Alloys Compd 613 (2014) 46–54.
[20] W. Xie, X. Tang, Y. Yan, Q. Zhang, T.M. Tritt, Unique nanostructures and enhanced thermoelectric performance of melt-spun BiSbTe alloys, Appl. Phys. Lett. 94 (2009) 102111.
[21] D.G. Zhao, X.Y. Li, W. Jiang, L.D. Chen, Fabrication of CoSb3/MoCu thermoelectric joint by one-step SPS and evaluation, J. Inorg. Mater. 24 (2009) 545–548.
[22] T. Lin, C. Liao, A.T. Wu, Evaluation of diffusion barrier between lead-free solder systems and thermoelectric materials, J. Electron. Mater. 41 (2012) 153–158.
[23] T. Sakamoto, Y. Taguchi, T. Kutsuwa, K. Ichimi, S. Kasatani, M. Inada, Investigation of barrier-layer materials for Mg2Si/Ni interfaces, J. Electron. Mater. 45 (2016) 1321–1327.
[24] C. Prahoveanu, L. Laversenne, C. de Vaulx, A. Bès, K. Azzouz, A. Lacoste, Investigation of diffusion barrier layers for Bi-Doped Mg2 (Si, Ge) thermoelectric legs, J. Electron. Mater. 45 (2016) 5570–5581.
[25] D. Gromov, Y.I. Shtern, M. Rogachev, A. Shulyat'ev, E. Kirilenko, M.Y. Shtern, V. Fedorov, M. Mikhailova, Mo/Ni and Ni/Ta–W–N/Ni thin-film contact layers for (Bi, Sb) 2Te3-based intermediate-temperature thermoelectric elements, Inorg. Mater. 52 (2016) 1132–1136.
[26] C.S. Chen, P. Yiu, C.L. Li, J.P. Chu, C.H. Shek, C.H. Hsueh, Effects of annealing on mechanical behavior of Zr–Ti–Ni thin film metallic glasses, Mater. Sci. Eng. A 608 (2014) 258–264.
[27] C.W. Wang, P. Yiu, J.P. Chu, C.H. Shek, C.H. Hsueh, Zr–Ti–Ni thin film metallic glass as a diffusion barrier between copper and silicon, J. Mater. Sci. 50 (2015) 2085–2092.
[28] M.H. Chuang, C. Wang, B.K. Chao, W.L. Kao, J.J. Shyue, C.H. Hsueh, Mechanical properties and microstructure of Zr-Ti-Ni thin film metallic glasses modified with minor SF_6, Compos. Part B 129 (2017) 243–250.
[29] W. Diyatmika, J.P. Chu, Y.W. Yen, W.Z. Chang, C.H. Hsueh, Thin film metallic glass as an underlayer for tin whisker mitigation: a room-temperature evaluation, Thin Solid Films 561 (2014) 93–97.
[30] C.H. Wang, H.H. Chen, P.Y. Li, P.Y. Chu, Kinetic analysis of Ni_5Zn_{21} growth at the interface between Sn–Zn solders and Ni, Intermetallics 22 (2012) 166–175.
[31] J. Oparowski, R. Sisson, R. Biederman, The effects of processing parameters on the microstructure and properties of sputter-deposited TiW thin film diffusion barriers, Thin Solid Films 153 (1987) 313–328.
[32] P. Ghate, J. Blair, C. Fuller, G. McGuire, Application of Ti: W barrier metallization for integrated circuits, Thin Solid Films 53 (1978) 117–128.
[33] H. Ramarotafika, G. Lemperiere, Influence of a DC substrate bias on the resistivity, composition, crystallite size and microstrain of WTi and WTi-N films, Thin Solid Films 266 (1995) 267–273.
[34] S. Bhagat, T. Alford, Texture formation in Ag thin films: effect of W–Ti diffusion barriers, J. Appl. Phys. 104 (2008) 103534.
[35] S. Bhagat, H. Han, T. Alford, Tungsten–titanium diffusion barriers for silver metallization, Thin Solid Films 515 (2006) 1998–2002.
[36] H. Lange, H. Reis, F. Fenske, AES study of the interaction of Ni and Al overlayers with W–Ti and W–Re diffusion barriers, Phys. Status Solidi (A) 115 (1989) 497–504.
[37] R. Nowicki, J. Harris, M.A. Nicolet, I. Mitchell, Studies of the Ti-W/Au metallization on aluminum, Thin Solid Films 53 (1978) 195–205.
[38] Q. Wang, S. Liang, Investigation on preparation and diffusion barrier properties of W–Ti thin films, Vacuum 85 (2011) 979–985.
[39] S. Berger, Elastic and plastic strains in Al/TiW/Si contacts during thermal cycles, Mater. Sci. Eng. A 288 (2000) 164–167.
[40] H. Wondergem, A. Heger, J. van Den Broek, Determination of W-Ti/Al thin-film interaction by sheet resistance measurement, Thin Solid Films 249 (1994) 6–10.
[41] A. Dirks, R. Wolters, A. Nellissen, On the microstructure-property relationship of WTi (N) diffusion barriers, Thin Solid Films 193 (1990) 201–210.
[42] S. Bhagat, N. Theodore, T. Alford, Thermal stability of tungsten–titanium diffusion barriers for silver metallization, Thin Solid Films 516 (2008) 7451–7457.
[43] W.P. Lin, C.C. Lee, Fluxless bonding of bismuth telluride chips to alumina using Ag–In system for high temperature thermoelectric devices, IEEE Trans. Compon. Packag. Manuf. Technol. (2011) 1311–1318.
[44] J.Y. Chang, R.S. Cheng, K.S. Kao, T.C. Chang, T.H. Chuang, Reliable microjoints formed by solid–liquid interdiffusion (SLID) bonding within a chip-stacking architecture, IEEE Trans. Compon. Packag. Manuf. Technol. (2012) 979–984.
[45] S. Fukumoto, K. Miyake, S. Tatara, M. Matsushima, K. Fujimoto, Solid-liquid interdiffusion bonding of copper using Ag-Sn layered films, Mater. Trans. 56 (2015) 1019–1024.
[46] B.K. Chao, S.C. Lin, L.W. Nien, J.H. Li, C.H. Hsueh, Effects of corner radius on periodic nanoantenna for surface-enhanced Raman spectroscopy, J. Optic. 17 (2015) 125002.
[47] M.H. Chien, L.W. Nien, B.K. Chao, J.H. Li, C.H. Hsueh, Effects of the rotation angle on surface plasmon coupling of nanoprisms, Nanoscale 8 (2016) 3660–3670.
[48] C. Okamura, T. Ueda, K. Hasezaki, Preparation of single-phase ZnSb thermoelectric materials using a mechanical grinding process, Mater. Trans. 51 (2010) 860–862.
[49] L. Kaufman, H. Nesor, Coupled phase diagrams and thermochemical data for transition metal binary systems—II, Calphad 2 (1978) 81–108.
[50] D.R. Brown, T. Day, K.A. Borup, S. Christensen, B.B. Iversen, G.J. Snyder, Phase transition enhanced thermoelectric figure-of-merit in copper chalcogenides, Apl. Mater. (2013) 052107.
[51] D.Y. Jung, K. Kurosaki, Y. Ohishi, H. Muta, S. Yamanaka, Effect of phase transition on the thermoelectric properties of Ag2Te, Mater. Trans. 53 (2012) 1216–1219.
[52] H. Yu, S. Dai, Y. Chen, Enhanced power factor via the control of structural phase transition in SnSe, Sci. Rep. 6 (2016) 26193.
[53] S. Petrović, D. Peruško, B. Gaković, M. Mitrić, J. Kovač, A. Zalar, V. Milinović, I. Bogdanović-Radović, M. Milosavljević, Effects of thermal annealing on structural and electrical properties of sputtered W–Ti thin films, Surf. Coating. Technol. 204 (2010) 2099–2102.
[54] R. Dronskowski, S. Kikkawa, A. Stein, Handbook of Solid State Chemistry, Wiley-VCH, 2017.